Available online at www.sciencedirect.com
SCIENCE DIRECT®
Journal of Magnetic Resonance 172 (2005) 168–175
JMR Journal of Magnetic Resonance
www.elsevier.com/locate/jmr

Frequency (250 MHz to 9.2 GHz) and viscosity dependence of electron spin relaxation of triarylmethyl radicals at room temperature

Rikard Owenius, Gareth R. Eaton, Sandra S. Eaton*

Department of Chemistry and Biochemistry, University of Denver, Denver, CO 80208, USA

Received 12 August 2004

Abstract

Electron spin relaxation times for four triarylmethyl (trityl) radicals at room temperature were measured by long-pulse saturation recovery, inversion recovery, and electron spin echo at 250 MHz, 1.5, 3.1, and 9.2 GHz in mixtures of water and glycerol. At 250 MHz T_1 is shorter than at X-band and more strongly dependent on viscosity. The enhanced relaxation at 250 MHz is attributed to modulation of electron–proton dipolar coupling by tumbling of the trityl radicals at rates that are comparable to the reciprocal of the resonance frequency. Deuteration of the solvent was used to distinguish relaxation due to solvent protons from the relaxation due to intra-molecular electron–proton interactions at 250 MHz. For trityl-CD_3, which contains no protons, modulation of dipolar interaction with solvent protons dominates T_1. For proton-containing radicals the relative importance of modulation of intra- and inter-molecular proton interactions varies with solution viscosity. The viscosity and frequency dependence of T_1 was modeled based on dipolar interaction with a defined number of protons at specified distances from the unpaired electron. At each of the frequencies examined T_2 decreases with increasing viscosity consistent with contributions from T_1 and from incomplete motional averaging of anisotropic hyperfine interaction.

Keywords: Triarylmethyl radicals; 250 MHz EPR; T_1; Electron spin relaxation; Modulation of dipolar coupling

1. Introduction

Triarylmethyl (trityl) radicals are being developed as EPR oximetry probes for in vivo spectroscopy and imaging [1–3]. Collisions with oxygen decrease relaxation times and increase continuous wave (CW) linewidths, and these changes can be calibrated to measure local oxygen concentration. To optimize probe design and to correctly distinguish changes due to oxygen from other factors that impact relaxation, it is important to understand the mechanisms of relaxation. Extensive studies of electron spin relaxation have been performed for immobilized samples at cryogenic temperatures, but much less is known about relaxation in fluid solution [4]. Studies of relaxation mechanisms for nitroxyl spin labels at or near room temperature have been performed by Freed and co-workers [5,6], Percival and Hyde [7], Robinson et al. [8,9], and Eaton and co-workers [10] and invoke contributions from modulation of nitrogen hyperfine interaction and g anisotropy by molecular tumbling, contributions from one or more thermally activated processes, and from spin rotation. The relative importance of these contributions depends on resonant frequency and molecular tumbling correlation times [10]. For semiquinones the dominant contributions to spin–lattice relaxation in fluid solution at X-band are spin rotation and a thermally activated process [11–14].

* Corresponding author. Fax: +1 303 871 2254.
E-mail address: sandra.eaton@nsm.du.edu (S.S. Eaton).

1090-7807/$ - see front matter © 2004 Elsevier Inc. All rights reserved.
doi:10.1016/j.jmr.2004.10.007

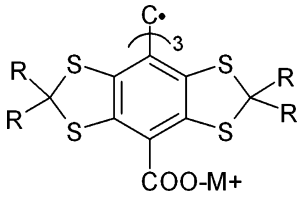

R = CD_3	trityl-CD_3
R = CH_3	trityl-CH_3
R = CH_2CH_2OH	OX63
R= $CH_2OCH_2CH_2OH$	OX31

Fig. 1. The triarylmethyl (trityl) radicals selected for this study have the same core structure and 12 identical R groups that are different for the 4 radicals. The cation, M^+, was Na^+.

For trityl radicals g values are about 2.0027 and g anisotropy is small [15], so spin rotation and modulation of g anisotropy are relatively ineffective relaxation mechanisms. Also there is not a large nuclear hyperfine interaction. Thus relaxation mechanisms for trityls are expected to be quite different than for nitroxyls or semiquinones. For trityl-CD_3 the temperature dependence of T_1 at X-band, and the weak dependence of room temperature T_1 on viscosity or on frequency between 1.5 and 9.2 GHz led to a proposal that the dominant contribution to T_1 in this frequency range was from a local vibrational mode [3]. To permit work with large lossy samples many in vivo experiments are performed at frequencies below 1 GHz so it is important to extend the relaxation time measurements to lower frequencies. It is also important to determine how the structure of the radical impacts the relaxation rates and mechanisms so the present study includes four trityl radicals that differ in the peripheral substituents (Fig. 1).

2. Experimental

2.1. Samples

Triarylmethyl (trityl) radicals trityl-CD_3, trityl-CH_3, OX63, and OX31 (Fig. 1) were provided by Nycomed [1]. Glycerol was of anhydrous grade (Aldrich Chemical, Milwaukee, WI), glycerol-d_8 was 99.7% isotopically enriched (CDN Isotopes, Que., Canada), and D_2O was 99.9% isotopically enriched (Cambridge Isotope Laboratories, Woburn, MA). Glycerol/water and glycerol-d_8/D_2O mixtures ranging from 10 to 90%, by volume were prepared gravimetrically based on a density of 1.26 g/mL for glycerol and glycerol-d_8. Trityl concentrations were 0.2 mM. This concentration is sufficiently low that radical–radical collisions make negligible contribution to spin relaxation [1,3], but high enough to get good signal-to-noise in the low-frequency measurements. Samples for X-band and S-band experiments were contained in thin-wall Teflon tubing with 1.15 mm i.d. and 1.35 mm i.d., respectively. The Teflon tubing was supported in a 4 mm o.d. quartz tube. Deoxygenation was performed by passing N_2 over the samples via a thin Teflon tube positioned in the quartz tube alongside the sample-containing Teflon tube until the relaxation times reached a limiting value. L-band samples were contained in 4 mm o.d. quartz tubes. Water samples were bubbled with N_2 to purge out oxygen and glycerol/water samples were degassed by multiple freeze–pump–thaw cycles. Samples for measurements at 250 MHz were contained in 10 mm pyrex NMR tubes. Deoxygenation of the samples was performed by bubbling N_2 into the sample. Sample tubes for L-band and 250 MHz experiments were flame-sealed.

2.2. EPR measurements

Measurements were performed at 20 ± 2 °C. X-band saturation recovery (SR) measurements of T_1 were made on a locally designed spectrometer [16]. X-band two-pulse electron spin echo (ESE) measurements of T_2 and three-pulse inversion recovery (IR)-ESE measurements of T_1 were performed on a previously described spectrometer [17,18] using an overcoupled modified Varian TE_{102} rectangular resonator. S- and L-band SR, two-pulse ESE and three-pulse IR-ESE measurements used locally designed S- and L-band spectrometers [19,20] with crossed-loop resonators (CLR) [19,21,22]. Each of the above resonators was designed to work with 4 mm o.d. tubes. Two-pulse ESE and three-pulse IR-ESE measurements at 250 MHz were made on a locally designed spectrometer [23] equipped with a CLR designed for 25 mm o.d. tubes [24] that was overcoupled to a Q of ~60. Dynamic Q-switching was used to minimize the dead time.

Long-pulse X-band SR measurements were performed at observe powers that were low enough that the recovery time constant was independent of observe power. Because the trityl EPR line is so narrow, it was fully excited in the IR-ESE experiment. Hence, the recovery was not affected by spectral diffusion, resulting in agreement, within uncertainty, between T_1 relaxation times obtained by SR and IR-ESE measurements. The reported X-band values are averages of results from SR and IR-ESE experiments. At X-, S-, and L-band, T_2 in the water and 50% glycerol samples is sufficiently long that T_1 was measured by IR-ESE. For the 90% glycerol samples T_2 is very short so T_1 was measured by SR. The 250 MHz spectrometer does not have an SR mode. For samples with sufficiently long T_2, T_1 was measured by IR-ESE. For the samples with $\geqslant$65% glycerol, the echo intensity at 250 MHz was too weak to measure two-pulse echo decays. However, T_1 values could be calculated from the dependence of the amplitude of the FID on τ in a π–τ–$\pi/2$, FID-IR pulse

sequence. SR, FID-IR, IR-ESE, and echo decay curves were corrected for instrumental artifacts by subtracting an off-resonance curve from the on-resonance curve. The data for all of the samples could be fit with single exponentials. The uncertainties in values of T_1 and T_2 are about 5–10%. In fluid solution the spin echo dephasing for the trityl radicals is dominated by spin–lattice relaxation and incomplete motional averaging of anisotropy, so the echo decay time constant is designated as T_2. Values are summarized in Tables 1 and 2.

2.3. Calculation of viscosity and rotational correlation time

For each of the water:glycerol compositions that was studied, the solvent viscosity was calculated based on values in the CRC Handbook (55th ed., p. D-206). The trityl tumbling correlation times (τ) were estimated from the Stokes–Einstein equation

$$\tau = \frac{4\pi\eta r^3}{3kT} = \frac{V\eta}{kT}, \tag{1}$$

where η is the solvent viscosity, r is the molecular radius, k is Boltzmann's constant, T is the temperature, and V is the molecular volume. The molecular volume was calculated from the molar mass, assuming a density of 0.9 g/cm^3. Use of this relationship between molar mass and molecular volume for trityl-CD_3, gives $r = 7.5$ Å, which is in good agreement with the value of $r = 7$ Å that was estimated by analysis of the spin echo dephasing by solvent protons [25]. The theory behind Eq. (1) assumes that the first layer of solvent molecules rotates with the solute, which is called the "stick" limit. To allow for variation in solute–solvent interaction a slip coefficient, C_{slip}, is introduced [26,27]

$$\tau = \frac{V\eta}{kT} C_{slip}. \tag{2}$$

Table 1
Electron spin relaxation times for trityls at 20 ± 2 °C[a]

Trityl	Frequency[b]	H_2O		50% glycerol		90% glycerol	
		T_1	T_2	T_1	T_2	T_1	T_2
Trityl-CD_3	X	17	11	17	3.7	19	0.24
	S	16	12	17	3.6	18	0.21
	L	14	12	15	3.7	17	0.21
	VHF	12	11	7.5	3.4	10[c]	—
Trityl-CH_3	X	16	9.1	17	1.8	17	0.18
	S	14	9.0	17	1.8	17	—
	L	12	8.9	13	1.7	15	—
	VHF	7.9	7.4	5.9	2.0	—	—
OX63	X	15	6.4	16	1.2	17	0.16
	S	14	6.6	16	1.2	17	—
	L	13	6.9	13	1.2	14	—
	VHF	6.2	5.3	6.3	1.4	—	—
OX31	X	14	5.1	15	1.1	16	0.13
	S	14	5.2	15	1.0	16	—
	L	12	5.5	13	1.1	14	—
	VHF	5.9	4.3	6.2	1.2	—	—

[a] Values are for deoxygenated samples. Relaxation times are in μs. H_2O/glycerol mixtures are described by v/v fractions.
[b] X-band measurements were made at 9.2 GHz, S-band at ca. 3.1 GHz, L-band at ca. 1.5 GHz, and VHF at ca. 250 MHz.
[c] 80% glycerol.

Table 2
Spin–spin relaxation times (T_2) for trityls at 250 MHz[a]

Trityl	H_2O	% glycerol					D_2O	% glycerol-d_8	
		10	20	35	50	65		20	35
Trityl-CD_3	11	9.8	7.4	5.5	3.4	1.6	14	—	12
Trityl-CH_3	7.4	6.0	4.7	3.2	2.0	1.3	8.8	6.3	4.6
OX63	5.3	4.3	3.6	2.2	1.4	—	5.6	4.0	3.1
OX31	4.3	3.7	3.0	2.0	1.2	—	4.4	—	2.5

[a] Values are for deoxygenated samples measured at 20 ± 2 °C. Relaxation times are in μs. H_2O/glycerol and D_2O/glycerol-d_8 mixtures are described by v/v fractions in %.

Values of C_{slip} are typically between 0 and 1 [27]. In aqueous solutions containing sucrose or glycerol, deviations from ideal Stokes–Einstein behavior tend to increase at high solute concentrations, τ becomes much smaller than predicted by Eq. (1), and C_{slip} decreases [9,28–30]. In this study the value of C_{slip} was an adjustable parameter.

2.4. Contributions to $1/T_1$

The trityl spin–lattice relaxation rates were modeled as the sum of contributions from a local mode, modulation of intra-molecular electron–proton dipolar interaction by tumbling of the trityl, and modulation of intermolecular electron–proton dipolar interaction by motion of solvation-sphere solvent molecules as shown in Eq. (3)

$$\frac{1}{T_1} = \frac{1}{T_1^{\text{local}}} + C_{\text{intra}} \frac{\tau_{\text{trityl}}}{1 + (\omega\tau_{\text{trityl}})^2} + C_{\text{solvent}} \times \frac{\tau_{\text{solvent}}}{1 + (\omega\tau_{\text{solvent}})^2}, \quad (3)$$

where $1/T_1^{\text{local}}$ is the frequency-independent contribution to the relaxation, ω is the resonance frequency in angular units ($2\pi\nu$), τ_{trityl} is the tumbling correlation time for the trityl, τ_{solvent} is the tumbling correlation time for the solvent, which was parameterized as $\tau_{\text{solvent}} = F\tau_{\text{trityl}}$, and C_{intra} and C_{solvent} are calculated as shown in Eqs. (4) and (5). The second and third terms on the right-hand side of Eq. (3) are the intra- and inter-molecular proton modulation contributions, respectively,

$$C_{\text{intra}} = n_1 \left(\frac{g_e g_n \beta_e \beta_n}{\hbar r_1^3} \right)^2 = n_1 \left(\frac{4.96 \times 10^8}{r_1^3} \right)^2 \text{s}^{-2}, \quad (4)$$

where n_1 is the number of interacting protons, r_1 is the average distance between the unpaired electron and the protons, g_e is the electron g value, g_n is the proton nuclear g value, and β_e and β_n are the electron and nuclear Bohr magneton

$$C_{\text{solvent}} = n_{\text{prot}} \left(\frac{g_e g_n \beta_e \beta_n}{\hbar r_{\text{solvent}}^3} \right)^2 = n_{\text{prot}} \left(\frac{4.96 \times 10^8}{r_{\text{solvent}}^3} \right)^2 \text{s}^{-2}, \quad (5)$$

where n_{prot} is the number of protons in a shell 5–5.5 Å thick, centered at an interspin distance of r_{solvent}. The thickness of the shell was adjusted to fit the experimental data. The thickness of the shell and the radius are not independent variables, and the resulting solutions are not unique. The modeling of the inter- and intra-molecular dipolar interactions is highly simplified and does not attempt to account for locations of individual protons. The goal of the modeling is to determine whether the magnitudes of the contributions to relaxation that are calculated for plausible interspin distances are sufficient to account for the observed changes in T_1 as a function of frequency and tumbling correlation times.

3. Results

3.1. Spin–lattice relaxation

The structures of the four trityl radicals for which relaxation times were measured are shown in Fig. 1. The radicals differ only in the peripheral substituents, R. The values of T_1 and T_2 in water, 50% glycerol, and 90% glycerol as a function of frequency are summarized in Table 1. For all four radicals the values of T_1 are significantly shorter at VHF (250 MHz) than at higher frequency. To elucidate the processes that contribute to the faster relaxation at lower frequency, data were recorded as a function of solvent viscosity, which was varied by changing the ratio of glycerol to water. At X-band there is little dependence of T_1 on viscosity (Fig. 2). However, at 250 MHz there is substantial variation in T_1 as a function of viscosity and the maximum relaxation rate occurs at different solvent compositions for different radicals (Fig. 2).

At 250 MHz in D_2O or 35% glycerol-d_8/D_2O the values of T_1 for trityl-CD_3 are 16.4 and 15.9 μs, respectively, which are similar to the values observed at higher microwave frequencies (Table 1), and are much longer than the 12.2 and 8.0 μs observed in H_2O or 35% glycerol, respectively, at 250 MHz. The increase in T_1 when solvent is deuterated indicates that solvent

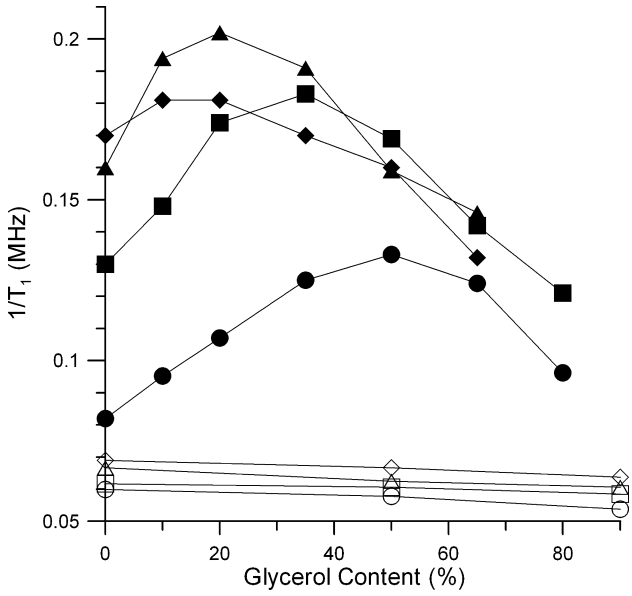

Fig. 2. Dependence of $1/T_1$ on solvent composition for trityl-CD_3 (○, ●), trityl-CH_3 (□, ■), OX63 (△, ▲), and OX31 (◇, ♦) at X-band (open symbols) and at 250 MHz (solid symbols). To emphasize trends solid lines connect the points.

protons play a significant role in the relaxation. Tumbling correlation times for trityl-CD_3 calculated using the Stokes–Einstein equation (Eq. (1)) are similar to $1/\omega$ at 250 MHz which makes modulation of electron–proton dipolar interaction by tumbling an efficient relaxation process. Since there are no protons in trityl-CD_3, the only protons that are available to effect relaxation are the solvent protons. Electron–nuclear dipolar interaction is proportional to the nuclear magnetic moment. The decrease of the nuclear magnetic moment by a factor of 6 from proton to deuteron is so large that relaxation due to dipolar interaction with deuterons was small relative to experimental uncertainties in these measurements. The intermolecular contribution to relaxation for trityl-CD_3 $(1/T_1 - 1/T_1^{\text{local}})$, is plotted in Fig. 3A as a function of the tumbling correlation times for the solvent protons. The thickness of the shell of interacting protons and average distance to the protons was adjusted to match the maximum amplitude of the contribution from solvent protons in Eq. (3) to the maximum value of $1/T_1^{\text{inter}}$. The value of C_{slip} (Eq. (2)) was adjusted to match the curve calculated for the intermolecular interactions to the experimental values of $1/T_1^{\text{inter}}$. Up to 50% glycerol good agreement was obtained for $C_{\text{slip}} = 0.21$ and the Stokes–Einstein tumbling

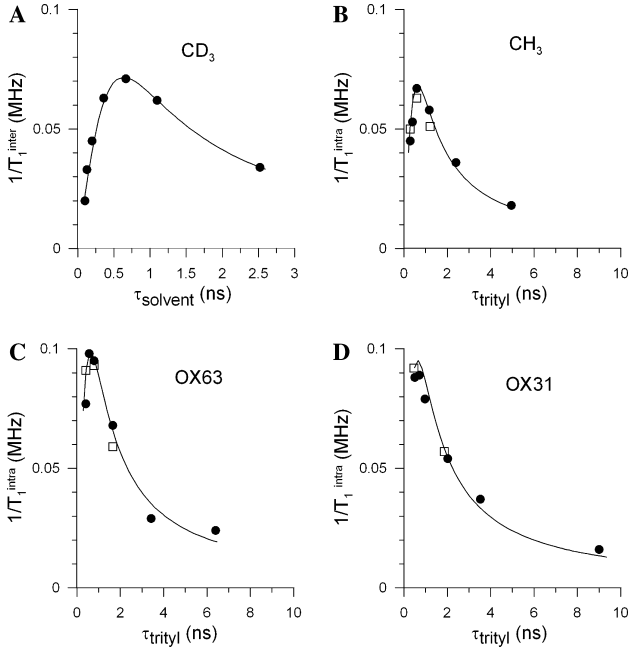

Fig. 3. Dependence of contributions to $1/T_1$ at 250 MHz on tumbling correlation times. (A) $1/T_1^{\text{inter}} = 1/T_1 - 1/T_1^{\text{local}}$ for trityl-CD_3 (●). $1/T_1^{\text{intra}} = 1/T_1 - 1/T_1^{\text{local}} - 1/T_1^{\text{inter}}$ for (B) trityl-CH_3, (C) OX63 or (D) OX31 in water:glycerol (●) or D_2O:glycerol-d_8 mixtures (□). The solution compositions are the same as in Fig. 2. In part (A) the correlation times shown on the x-axis are for solvent protons. In parts (B–D) the correlation times shown on the x-axes are for the trityl radical. The solid lines are the fits to the individual contributions that were obtained with the model discussed in the text (Eq. (3)) and the parameters summarized in Table 3.

correlation times of trityl-CD_3. At 65 and 80% glycerol $C_{\text{slip}} = 0.10$ and 0.07, respectively. The smaller values of C_{slip} at higher glycerol concentration are consistent with prior studies of the limitations of the Stokes–Einstein model [9,28–30].

The relaxation rates for trityl-CH_3 as a function of viscosity at 250 MHz (Fig. 2) were significantly different than for trityl-CD_3, which indicates that modulation of intra-molecular electron–proton dipolar interaction also contributes to the relaxation. For each glycerol/water mixture the intra-molecular contribution to $1/T_1$ for trityl-CH_3 (Fig. 3B) was calculated as $1/T_1^{\text{intra}} = 1/T_1 - 1/T_1^{\text{local}} - 1/T_1^{\text{inter}}$, where $1/T_1^{\text{local}}$ is the frequency-independent contribution and $1/T_1^{\text{inter}}$ is the contribution from solvent protons to the relaxation of trityl-CD_3 (Fig. 3A). To test the validity of this approach to separating contributions, values of T_1 in glycerol-d_8/D_2O mixtures also were obtained. For the deuterated solvents $1/T_1^{\text{intra}} = 1/T_1 - 1/T_1^{\text{local}}$. The values of $1/T_1^{\text{intra}}$ obtained in the natural isotope abundance solvents and in the deuterated solvents are in good agreement (Fig. 3B). To calculate the coefficient C_{intra} (Eq. (4)) the number of protons (n_1) was fixed at 36 and the interspin distance, r_1, was adjusted to match the maximum in $1/T_1^{\text{intra}}$. The value of C_{slip} in Eq. (2) was adjusted to obtain agreement between the curve calculated for intra-molecular interaction and the experimental data points (Fig. 3, Table 3).

The intra-molecular contributions to $1/T_1$ for OX63 and OX31 were analyzed by a procedure analogous to that for trityl-CH_3 except that two shells of protons were included in the calculation of the intra-molecular interaction (Eq. (4)). Also, the intermolecular interaction with solvent protons for OX63 and OX31 was assumed to be 0.9 or 0.8, respectively, times that for trityl-CD_3 because of the larger sizes of the molecules. For both OX63 and OX31 there is good agreement between the values of $1/T_1^{\text{intra}}$ calculated by subtraction of the contribution of solvent protons in natural isotope abundance solvents and values found in deuterated solvents (Figs. 3C and D). The parameters that were used to obtain the fit lines are summarized in Table 3.

For trityl-CD_3 the x-axis in Fig. 3A is the solvent tumbling correlation time. The intermolecular contribution to relaxation is maximum when $\tau_{\text{solvent}} = 1/\omega = 0.63$ ns, which occurs in approximately 50% glycerol. For the proton-containing trityls the x-axes in Figs. 3B–D are the tumbling correlation times for the trityls. For the same solvent composition the trityl tumbling correlation time increases with increasing molar mass, i.e., trityl-CH_3 < OX63 < OX31. The maximum in $1/T_1^{\text{intra}}$ occurs at $\tau_{\text{trityl}} = 0.63$ ns for each of the trityls but that tumbling correlation time occurs in about 20% glycerol for trityl-CH_3, about 10% glycerol for OX63 and about 5% glycerol for OX31 (Figs. 2 and 3).

Table 3
Fitting parameters

Trityl	MW[a]	$\frac{1}{T_1^{local}}$[b] (s^{-1})	r_1 (n_1)[c] (Å)	r_2 (n_2)[d] (Å)	$r_{solvent}$[e] (Å)	C_{slip}[f]	F[g]
trityl-CD_3	1010	0.59×10^5			8.2	0.21	
trityl-CH3	975	0.61×10^5	5.9 (36)		8.2	0.65	0.28
OX63	1335	0.66×10^5	5.3 (24)	7.2 (24)	8.4	0.68	0.22
OX31	1695	0.66×10^5	5.3 (24)	7.5 (24)	8.4	0.65	0.15

[a] Molecular weight for radical, not including cations.
[b] Contribution to relaxation from local mode.
[c] Average distance to first set of proton in molecule; number of protons in set.
[d] Average distance to second set of protons in molecule; number of protons in set.
[e] Average radius of shell of solvent protons with thickness of 5–5.5 Å.
[f] Slip coefficient (multiplier of Stokes–Einstein tumbling correlation time) for solutions with glycerol up to 50%. For trityl-CD_3 this value relates the effective tumbling correlation time for solvent protons to the Stokes–Einstein value for the trityl.
[g] Ratio of tumbling correlation time for solvent to tumbling correlation time for trityl.

The contributions to relaxation from all of the processes are combined in the plots shown in Fig. 4. The importance of the intermolecular contributions is highlighted by the differences between values of $1/T_1$ in natural abundance solvents (●) and deuterated solvents (□). The plot for trityl-CD_3 (Fig. 4A) differs from that in Fig. 3A only in the addition of $1/T_1^{local}$, which is independent of $\tau_{solvent}$. As in Fig. 3, the *x*-axes in Figs. 4B–D are the tumbling correlation times for the trityls. For each solvent composition, the tumbling correlation time for the solvent, $\tau_{solvent}$, is shorter than τ_{trityl}. The tumbling correlation times of the solvent protons were expressed as a fraction (F) of the values for the trityl. The maximum intermolecular effect ($\tau_{solvent} = 0.63$ ns) occurs in approximately 50% glycerol and τ_{trityl} is about 2, 3, and 4 ns for trityl-CH_3, OX63, and OX31, respectively, in solvent with this composition. Thus inclusion of the intermolecular contribution causes the shapes of the plots in Fig. 4B–D to be quite different than the corresponding ones in Fig. 3.

The frequency dependence of $1/T_1$ for the four trityl radicals is shown in Fig. 5. The same fit parameters that were used to obtain the calculated curves in Figs. 3 and 4 (Table 3) also give good agreement with the observed frequency dependence.

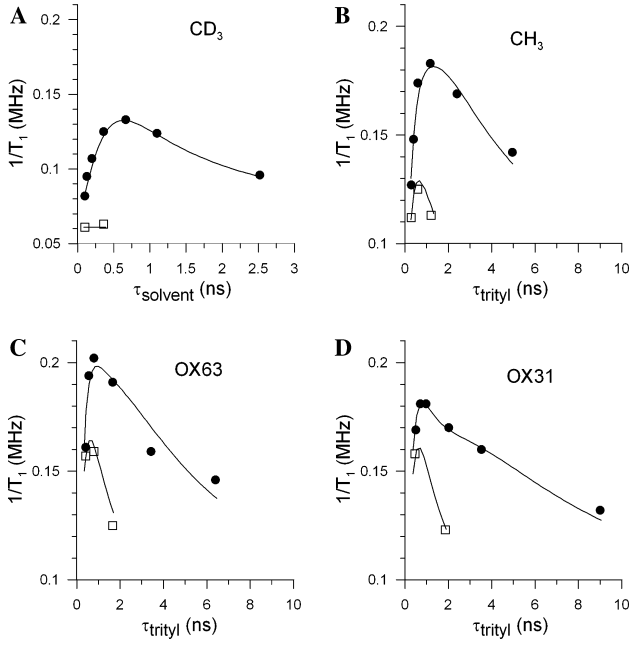

Fig. 4. Dependence of $1/T_1$ at 250 MHz on tumbling correlation times for (A) trityl-CD_3, (B) trityl-CH_3, (C) OX63, and (D) OX31 in water:glycerol (●) or D_2O:glycerol-d_8 mixtures (□). In part (A) the correlation times shown on the *x*-axis are for solvent protons. In parts (B–D) the correlation times shown on the *x*-axes are for the trityl radical and the correlation times for solvent protons are F (Table 3) times that for the trityl. In normal isotope abundance solvents the fit lines (___) include contributions from a local mode plus modulation of intra-molecular and inter-molecular (radical-solvent) electron–proton interactions (Eq. (3)). In deuterated solvents there is no contribution to the fit line (___) from solvent protons. The parameters used in the fitting are shown in Table 3.

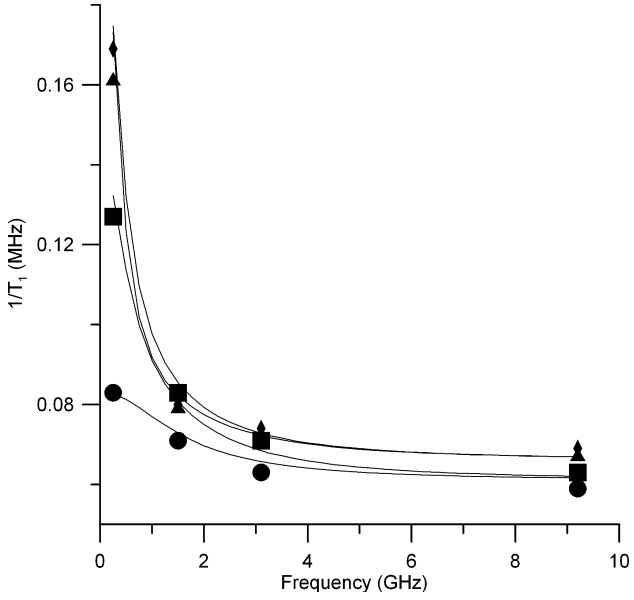

Fig. 5. Frequency dependence of $1/T_1$ for trityl-CD_3 (●), trityl-CH_3 (■), OX63 (▲), and OX31 (♦) in water. The fit lines (___) were obtained with the same parameters as used for the samples in normal isotope abundance solvents (Fig. 4, Table 3).

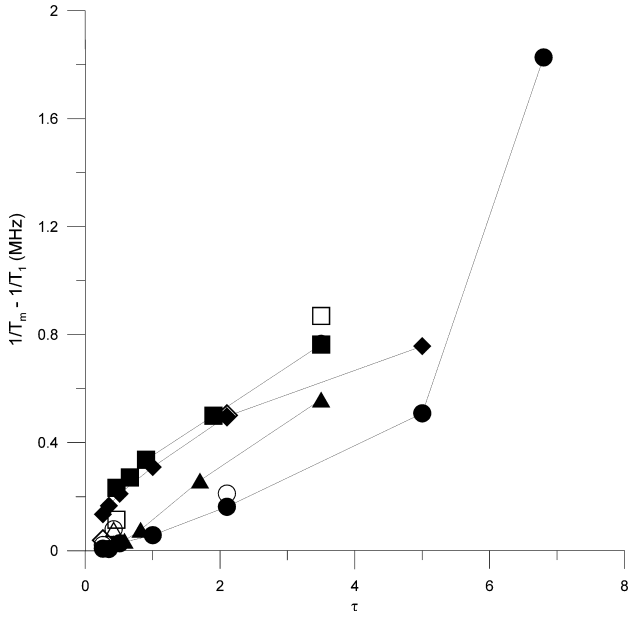

Fig. 6. Contributions to $1/T_2$ from incomplete motional averaging of anisotropic interactions as a function of tumbling correlation time for trityl-CD_3 (○, ●), trityl-CH_3 (□, ■), OX63 (△, ▲), and OX31 (◇, ♦). The closed symbols are values at 250 MHz, and the open symbols are averages of data at L, S-, and X-band. The lines connect the points.

3.2. Spin–spin relaxation

The values of T_2 in Tables 1 and 2 vary both with frequency and solvent composition. In solutions with low-glycerol concentrations the similarity of values of T_1 and T_2 indicates that T_1 accounts for a substantial fraction of T_2. To analyze trends in other contributions to T_2, values of $1/T_2 - 1/T_1$ are plotted as a function of τ_{trityl} in Fig. 6. The contributions shown in Fig. 6 increase as the tumbling correlation rate slows as expected for incomplete motional averaging of anisotropic interactions. The averages of values of $(1/T_2 - 1/T_1)$ for data at X-band, S-band, and L-band are similar to the values at 250 MHz, which indicates that the anisotropies that are averaged are from hyperfine interactions rather than g anisotropy.

4. Discussion

In a discussion of spin–lattice relaxation mechanisms for nitroxyl radicals in fluid solution it was proposed that modulation of dipolar coupling between the unpaired electron and solvent protons contributed [8]. However, this contribution was subsequently ruled out when it was shown that deuteration of the solvent did not impact the nitroxyl T_1 [10]. The results obtained in the current studies demonstrate that modulation of both inter- and intra-molecular electron–proton dipolar coupling by molecular tumbling makes significant contributions to spin–lattice relaxation for trityl radicals at 250 MHz. The contribution from modulation of proton interactions is more significant for the trityl radicals than for the nitroxyl radicals because several of the contributions that dominate for the nitroxyl radicals are not present for the tritys. This contribution is largest for tritys at operating frequencies near 250 MHz because τ_{trityl} is approximately $1/\omega$.

To model the spin–lattice relaxation rates it was necessary to introduce a slip-coefficient correction into the Stokes–Einstein equation (Eq. (2)). The coefficients for the three proton-containing tritys were in the range of 0.65–0.68 (Table 3) for solvent compositions up to 50% glycerol. The similarity in the slip coefficients for the three radicals indicates that the solute–solvent interaction is similar for the three molecules, as would be expected based on the three carboxylate groups in each of the tritys. The similarity between trityl-CH_3, which does not contain hydroxyl groups and OX63 and OX31, which contain hydroxyl groups, suggests that the hydroxyl groups do not dominate the interactions that determine C_{slip}.

A very simple model of the electron–proton dipolar interaction was used to test whether the magnitude of the interaction was sufficient to explain the relaxation effects. The average distance to the protons of the methyl groups (r_1) of trityl-CH_3 are slightly longer than the distances to the nearest methylene protons of OX63 or OX31 (Table 3), which is consistent with expectations that in the preferred conformations, the bulky substituents are pointed away from the radical center. Values of r_1 about 5.3–5.9 Å are consistent with conformations calculated by simple energy minimization performed with PC Spartan (WaveFunction, Irvine, CA). For OX63 and OX31 the more distant sets of methylene protons at distance r_2 contribute very little to the spin relaxation so a substantial range of r_2 values could be used in the modeling.

Acknowledgments

The trityl radicals were a generous gift from Nycomed Innovations AB to Professor Howard Halpern, University of Chicago, who supplied the samples for this study. We thank Richard W. Quine and Professor George A. Rinard for their support and expertise concerning the operation of spectrometers and resonators. This work was supported by NIBIB EB002807 and P41-EB002034.

References

[1] J.H. Ardenkjaer-Larsen, I. Laursen, I. Leunbach, G. Ehnholm, L.-G. Wistrand, J.S. Petersson, K. Golman, EPR and DNP

properties of certain novel single electron contrast agents intended for oximetric imaging, J. Magn. Reson. 133 (1998) 1–12.
[2] T.J. Reddy, T. Iwama, H.J. Halpern, V.H. Rawal, General synthesis of persistent trityl radicals for EPR imaging of biological systems, J. Org. Chem. 67 (2002) 4635–4639.
[3] L. Yong, J. Harbridge, R.W. Quine, G.A. Rinard, S.S. Eaton, G.R. Eaton, C. Mailer, E. Barth, H.J. Halpern, Electron spin relaxation of triarylmethyl radicals in fluid solution, J. Magn. Reson. 152 (2001) 156–161.
[4] S.S. Eaton, G.R. Eaton, Relaxation times of organic radicals and transition metal ions, Biol. Magn. Reson. 19 (2000) 29–154.
[5] S.A. Goldman, G.V. Bruno, J.H. Freed, ESR studies of anisotropic rotational reorientation and slow tumbling in liquid and frozen media. II. Saturation and nonsecular effects, J. Chem. Phys. 59 (1973) 3071–3091.
[6] J.S. Hwang, R.P. Mason, L.-P. Hwang, J.H. Freed, Electron spin resonance studies of anisotropic rotational reorientation and slow tumbling in liquid and frozen media. III. Perdeuterated 2,2,6,6-tetramethyl-4-piperidone-*N*-oxide and an analysis of fluctuating torques, J. Phys. Chem. 78 (1975) 489–511.
[7] P.W. Percival, J.S. Hyde, Saturation-recovery measurements of the spin-lattice relaxation times of some nitroxides in solution, J. Magn. Reson. 23 (1976) 249–257.
[8] B.H. Robinson, D.A. Haas, C. Mailer, Molecular dynamics in liquids: spin-lattice relaxation of nitroxide spin labels, Science 263 (1994) 490–493.
[9] B.H. Robinson, C. Mailer, A.W. Reese, Linewidth analysis of spin labels in liquids. II. Experimental, J. Magn. Reson. 138 (1999) 210–219.
[10] R. Owenius, G.E. Terry, M.J. Williams, S.S. Eaton, G.R. Eaton, Frequency dependence of electron spin relaxation of nitroxyl radicals in fluid solution, J. Phys. Chem. B 108 (2004) 9475–9481.
[11] S.K. Rengen, M.P. Khakhar, B.S. Prabhananda, B. Venkataraman, Electron spin–lattice relaxation in organic free radicals in solutions, Pure Appl. Chem. 32 (1972) 287–305.
[12] S.K. Rengen, M.P. Khakhar, B.S. Prabhananda, B. Venkataraman, Study of molecular motions in liquids by electron spin–lattice relaxation measurements, I. Semiquinone ions in hydrogen bonding solvents, Pramana 3 (1974) 95–121.
[13] S.K. Rengen, M.P. Khakhar, B.S. Prabhananda, B. Venkataraman, Study of molecular motions in liquids by electron spin-lattice relaxation measurements, II. 2,5-Di-tert-butylsemiquinone ions in acetonitrile and tetrahydrofuran, J. Magn. Reson. 16 (1974) 35–43.
[14] B.S. Prabhananda, J.S. Hyde, Study of molecular motions in liquids by electron spin relaxation: halogenated *p*-semiquinone anions in alcohols, J. Chem. Phys. 85 (1986) 6705–6712.
[15] A.J. Fielding, W.P. Carl, G.R. Eaton, S.S. Eaton, Multifrequency EPR of four triarylmethyl radicals, Appl. Magn. Reson. (2004), in press.
[16] R.W. Quine, S.S. Eaton, G.R. Eaton, Saturation recovery electron paramagnetic resonance spectrometer, Rev. Sci. Instrum. 63 (1992) 4251–4262.
[17] R.W. Quine, G.R. Eaton, S.S. Eaton, Pulsed EPR spectrometer, Rev. Sci. Instrum. 58 (1987) 1709–1723.
[18] G.A. Rinard, R.W. Quine, J.R. Harbridge, R. Song, G.R. Eaton, S.S. Eaton, Frequency dependence of EPR signal-to-noise, J. Magn. Reson. 140 (1999) 218–227.
[19] R.W. Quine, G.A. Rinard, B.T. Ghim, S.S. Eaton, G.R. Eaton, A 1–2 GHz pulsed continuous wave electron paramagnetic resonance spectrometer, Rev. Sci. Instrum. 67 (1996) 2514–2527.
[20] G.A. Rinard, R.W. Quine, R. Song, G.R. Eaton, S.S. Eaton, Absolute EPR spin echo and noise intensities, J. Magn. Reson. 140 (1999) 69–83.
[21] G.A. Rinard, R.W. Quine, B.T. Ghim, S.S. Eaton, G.R. Eaton, Easily tunable crossed-loop (bimodal) EPR resonator, J. Magn. Reson. A 122 (1996) 50–57.
[22] G.A. Rinard, R.W. Quine, B.T. Ghim, S.S. Eaton, G.R. Eaton, Dispersion and superheterodyne EPR using a bimodal resonator, J. Magn. Reson. A 122 (1996) 58–63.
[23] R.W. Quine, G.A. Rinard, S.S. Eaton, G.R. Eaton, A pulsed and continuous wave 250 MHz electron paramagnetic resonance spectrometer, Magn. Reson. Eng. 15 (2002) 59–91.
[24] G.A. Rinard, R.W. Quine, G.R. Eaton, S.S. Eaton, 250 MHz crossed loop resonator for pulsed electron paramagnetic resonance, Magn. Reson. Eng. 15 (2002) 37–46.
[25] A. Zecevic, G.R. Eaton, S.S. Eaton, M. Lindgren, Dephasing of electron spin echoes for nitroxyl radicals in glassy solvents by non-methyl and methyl protons, Mol. Phys. 95 (1998) 1255–1263.
[26] D. Kivelson, P. Madden, Light scattering studies of molecular liquids, Annu. Rev. Phys. Chem. 31 (1980) 523–558.
[27] M.J.G.W. Roozen, M.A. Hemminga, Molecular motion in sucrose-water mixtures in the liquid and glassy state as studied by spin probe ESR, J. Phys. Chem. 94 (1990) 7326–7329.
[28] T.K. Hitchens, R.G. Bryant, Nonideal response of rotational correlation times of $[La(EDTA)]^-$ and $[Co(en)_3]^{3+}$ in aqueous glycerol and sucrose solutions, J. Phys. Chem. 99 (1995) 5612–5615.
[29] M.I. Sluch, M.M. Somoza, M.A. Berg, Friction on small objects and the breakdown of hydrodynamics in solution: rotation of anthracene in poly(isobutylene) from small-molecule to polymer limits, J. Phys. Chem. B 106 (2002) 7385–7397.
[30] P.S. Belton, L.H. Sutcliffe, D.G. Gillies, X. Wu, A.I. Smirnov, A new water-soluble and lipid-insoluble spin probe: application to the study of aqueous sucrose solutions, Magn. Reson. Chem. 37 (1999) 36–42.